Article **Journal Renewable Energy**
December, 2023 Vol.7 No.19 28-37

Geothermal energy harnessing using a horizontal composite geothermal heat exchanger and a vertical geothermal heat exchanger

Aprovechamiento de la energía geotérmica utilizando un intercambiador de calor geotérmico compuesto horizontal y un intercambiador de calor geotérmico vertical

RUBIO-LÓPEZ, Osvaldo†*, MONTOYA-SANTIYANES, Luis Alvaro, GARCÍA-GUENDULAIN, Juan Manuel and MENDOZA-ROJAS, América Eileen

Universidad Politécnica de Querétaro, El Marques, Queretaro 76240, Mexico

ID 1st Author: *Osvaldo, Rubio-López* / **ORC ID**: 0000-0002-9073-8249, **CVU CONAHCYT ID**: 484537

ID 1st Co-author: *Luis Alvaro, Montoya-Santiyanes* / **ORC ID**: 0000-0003-3380-1544, **CVU CONAHCYT ID**: 492895

ID 2nd Co-author: *Juan Manuel, García-Guendulain* / **ORC ID**: 0000-0001-5636-5074, **CVU CONAHCYT ID**: 514795

ID 3rd Co-author: *América Eileen, Mendoza-Rojas* / **ORC ID**: 0000-0003-5636-5074, **CVU CONAHCYT ID**: 854644

DOI: 10.35429/JRE.2023.19.7.28.37 Received July 03, 2023; Accepted November 30, 2023

Abstract

Heat exchangers in combination with geothermal heat pumps (GHP) have been growing in HVAC and sanitary applications, as well as associated research. Therefore, in this work, a Composite Geothermal Heat Exchanger (CGHE) and a Horizontal Geothermal Heat Exchanger (HGHE) were designed and fabricated Through experimental tests and simulation in ANSYS-CFX, the behavior of the temperature of the refrigerant fluid inside the exchangers was compared. The geometry of the CGHE was based on a Vertical Geothermal Heat Exchanger (VGHE) with the installation depth of an HGHE. Water at different temperatures was used as the cooling fluid with a mass flow equal to 0.26 L/s for the experimental tests and simulations in ANSYS-FLUENT for both the CGHE and HGHE. The CGHE and HGHE were installed within a volume of 3.25 m^3 of ground. The experiments and simulations in ANSYS-CFX showed that the refrigerant fluid inside the CGHE exhibit a greater use of geothermal energy because it increases and reduces the temperature of the refrigerant more quickly compared to the HGHE.

Energy, Geothermal, Exchanger

Resumen

Los intercambiadores de calor en combinación con las bombas de calor geotérmicas han demostrado un crecimiento en aplicaciones sanitarias y de climatización, así como investigaciones asociadas. Por lo tanto, en este trabajo se diseñó y construyó un Intercambiador de Calor Geotérmico Compuesto (ICGC) y un Intercambiador de Calor Geotérmico Horizontal (ICGH). A través de pruebas experimentales y simulación en ANSYS-CFX se comparó el comportamiento de la temperatura del fluido refrigerante en el interior de los intercambiadores. La geometría del ICGC fue basada en un Intercambiador de Calor Geotérmico Vertical (ICGV) con la profundidad de instalación de un ICGH. Se utilizó agua como refrigerante variando la temperatura, y un flujo másico igual a 0.26 L/s fue utilizado tanto en los experimentos como en las simulaciones para ambos intercambiadores. El ICGC y el ICGH fueron instalados dentro de un volumen de 3.25 m^3 de tierra. Los experimentos y la simulación en ANSYS-CFX mostraron que el fluido refrigerante dentro del ICGC presenta un aprovechamiento mayor de la energía geotérmica debido a que incrementa y reduce más rápido la temperatura del fluido refrigerante en comparación al ICGH.

Energía, Geotermia, Intercambiador

Citation: RUBIO-LÓPEZ, Osvaldo, MONTOYA-SANTIYANES, Luis Alvaro, GARCÍA-GUENDULAIN, Juan Manuel and MENDOZA-ROJAS, América Eileen. Geothermal energy harnessing using a horizontal composite geothermal heat exchanger and a vertical geothermal heat exchanger. Journal Renewable Energy. 2023. 7-18: 28-37

* Author Correspondence (e-mail: osvaldo.rubio@upq.edu.mx)
† Researcher contributing as first author.

1. Introduction

A Geothermal Heat Pump (GHP) extracts the thermal energy from underground by means of a Geothermal Heat Exchanger (GHE), and through that energy supply evaporates a cooling fluid at very low pressure and temperature that is compressed through a compressor, thus increasing its temperature and pressure. The steam then passes to the condenser and gives heat to the medium to heat. Finally, the fluid passes through an expansion valve, reducing its temperature and pressure again and restarting the refrigeration cycle (Mustafa, 2008).

This provides significant energy savings of between 30% and 70% compared to conventional cooling and heating systems (Benli & Durmus, 2009). Heat exchangers hold a pivotal role in process production, chiefly segmented into four groups based on heat transfer principles (Gong *et al*., 2023) direct contact heat exchangers (Zheng *et al*., 2022), accumulator heat exchangers (Chen *et al.*, 2022) surface heat exchangers (Triki *et al*., 2021), and inter-wall heat exchangers (Guo *et al*., 2014), with the latter being most prevalent in industrial use and having received comprehensive examination (Lv *et al.*, 2018).

The first known records that are held in using the land as a heat source using a GHP is a Swiss patent issued and registered in the year 1912 (Philippe *et al*., 2011) However, with the development of the classical heat conduction theory (ground-pipe) proposed by Ingersoll and Plass in 1948, as well as the analytical basic theory for heat conduction in GHP systems also proposed by Ingersoll and Plass (Ingersoll *et al*., 1950; Rousseau *et al*., 2017).

Over the past two decades, major efforts have been made to establish standards for the installation and development of GHE design methods by the International Geothermal Ground Source Heat Pump Association (IGSHPA, 2013; Eskilson, 1987; Rees, 2016; IGSHPA, 2018). It is estimated that GHP's facilities have grown continuously worldwide, with an annual interval between 10% and 30% in recent years (Fundación de la Energía de la Comunidad de Madrid, 2010).

GHEs make use of geothermal energy stored in the subsoil, classified as energy at very low temperature (T<30ºC), this energy can be used for heating, air conditioning and domestic hot water, making use of a GHP (Bose et al., 1985). (Yang *et al*., 2009) VGHEs have a geometric configuration in U or double U, with an internal diameter pipe that ranges between 19 mm and 38 mm, and each borehole for the installation of the VGHE has a depth ranging from 20 m to 200 m with a diameter ranging from 100 mm to 200 mm (Philippe *et al*., 2011).

To perform these functions, the GHP uses an HGHE and a VGHE, see Figure 1a and 1b (Mustafa *et al*., 2008; IGSHPA, 2018).

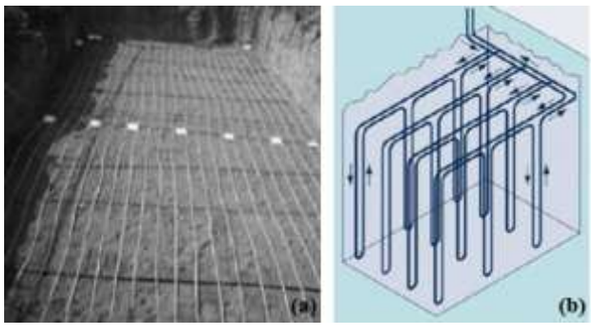

Figure 1 An HGHE installed in the subsoil at a depth of 2 meters
Huseyin Benli[a], Aydın Durmus[b], 2008

The article is mainly structured as follows: Section 2 shows the methodologies used to estimate the lengths of the exchangers and the selection of subsoil temperatures at different depths. In Section 3, the experiments and numerical simulations carried out to find the temperature distributions are specified. Section 4 specifies discussions and conclusions.

2. Metodology

2.1. Calculation of CGHE and HGHE lengths

The Composite Geothermal Heat Exchanger (CGHE) and HGHE of 15.8 m length with PEAD4710 high density polyethylene pipe were designed and built. CGHE and HGHE were installed in a subsoil external control volume equal to 3.25 m^3 of ground (see Figure 2) and in a subsoil control volume equal to 3.25 m^3 of ground (see Figure 3). The CGHE combines the geometry of a VGHE and the installation depths of a HGHE.

ISSN 2523-2881

The temperature behavior of the refrigerant fluid that circulates inside the GHEs was studied through six experimental tests and simulations in the ANSYS-FLUENT software, where water is considered as the refrigerant fluid subjected to different working temperatures.

The lengths for the CGHE and HGHE geometries was calculated according to the IGSHPA. The model established by the IGSHPA (IGSHPA, 2009) is based on Kelvin's linear heat source theory with some simplified assumptions. By using this method and the Equation (1), the total lengths are calculated considering the month with the lowest temperature recorded in the city of Santiago de Queretaro, Mexico, 2021.

$$L_H = \frac{Capacity_C\left(\frac{COP_C+1}{COP_C}\right)(R_P+R_S \cdot F_H)}{T_{max}-T_{s,m}} \quad (1)$$

where R_s represents the thermal resistance of the ground which is taken from Table 1, referring to a Vertisol type soil (National Institute of Geographical and Informatics Statistics, INEGI 2007), R_p is the thermal resistance of the pipe from CGHE and HGHE, F_H is the GHP operating factor, $Capacity_C$ is the refrigeration capacity, $T_{s,m}$, is the average temperature of the ground at a set depth, and T_{max} is the maximum temperature at the inlet of the refrigerant fluid to the GHP.

By substituting the values of the variables in Equation (1), the total length for the CGHE and HGHE is obtained, $L_H = 15.75\, m$ which turned out to be the same for both models.

The experiments were carried out at the CGHE and HGHE under two different boundary conditions. Figure 2 shows the first boundary condition, at which the external volume to the subsoil equal to 3.25 m^3 was fabricated and that is where the models were installed to perform the tests with water as refrigerant at different working temperatures.

Figure 2 First boundary condition with the external volume to the subsoil

For the second boundary condition, the same volume of 3.25 m^3 was considered but now excavated underground, and in this excavation the CGHE and HGHE were installed. The same experimental tests considering water as a refrigerant at different temperatures were carried out (see Figure 3).

Figure 3 Second boundary condition with the volume excavated in the subsoil

In the experimental tests, the next parameters were monitored for the refrigerant fluid: outlet speed, the temperatures at the inlet and outlet, and mass flow. The mass flow was used to estimate pressure losses within the geometry of the CGHE and HGHE.

Figure 4 shows the geometry of the CGHE with the length of 15.8 m according to the results obtained with Equation 1.

ISSN 2523-2881

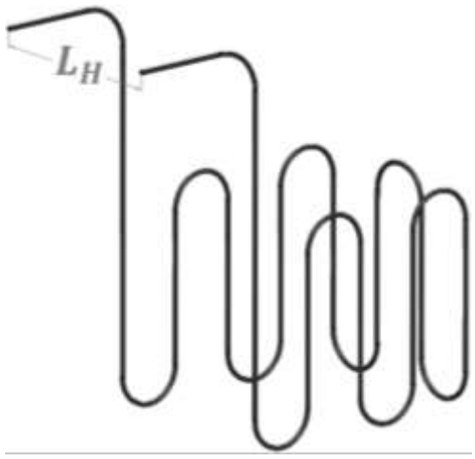

Figure 4 CGHE geometry

Figure 5 shows the geometry of the HGHE with the length of 15.8 m according to the results obtained with Equation 1.

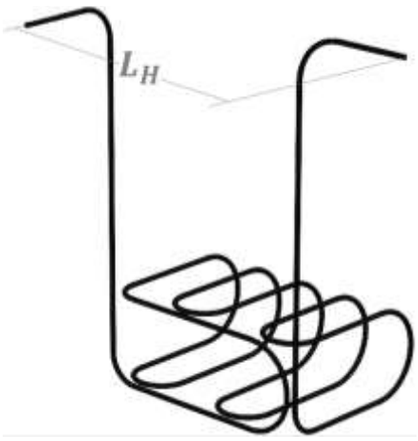

Figure 5 HGHE geometry

According to data from National Institute of Geographical and Informatics Statistics (INEGI, 2007; Consejo de Ciencia y Tecnología del Estado de Querétaro [CONCYTEQ], 2002) topographic data from the city of Santiago de Queretaro, Mexico, it is shown that Vertisol-type soils predominate, a soil with a high clay content classified as red or pottery clay and as light or semi-dry soil (INEGI, 2007).

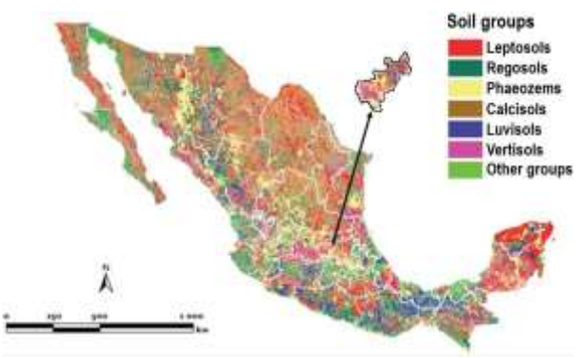

Figure 6 Classification of soil in Mexico, specifically in city of Queretaro

Table 1 contains the main thermophysical properties of Vertisol-type soil (INEGI, 2021).

Properties	Value
Thermal conductivity (λ)	0.46 W/m·ºC
Density (ρ)	2000 Kg/m^3
Specific heat (C_P)	879 J/Kg·ºC
Thermal diffusivity (α)	2.6166 x 10^{-7} m^2/s

Table 1 Thermophysical properties of a Vertisol-type soil

2.2. Temperature behavior in the city of Queretaro, Mexico

The city of Santiago de Queretaro is located at 20° 35' North latitude, with a longitude of 100° 23' West and an altitude of 1820 m s. n. m. (National Institute of Geographical and Informatics Statistics (INEGI 2007). The temperature recorded during 2021 was decisive to calculate the behavior of refrigerant fluid temperature in both models CGHE and HGHE. Graph 1 shows the behavior of the maximum, minimum and average temperatures (Meteored, 2023). (Data collected by the closest weather stations to the Queretaro International Airport (MMQT)).

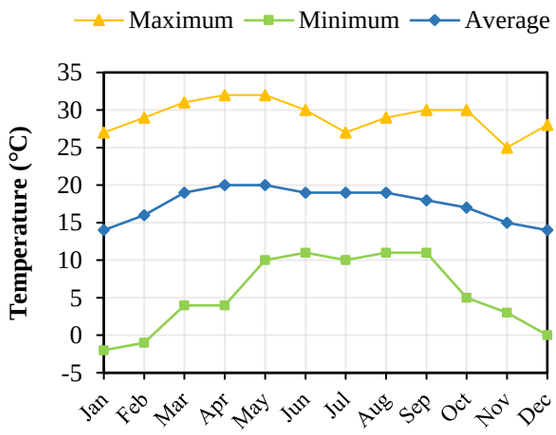

Graph 1 Behavior of maximum, minimum and average temperatures

2.3. Annual Oscillation of Surface Temperature (AOs)

The AOs is determined by using Equation 2. (Kusuda & Achenbach, 1965).

$$AOs = \left(\underset{Monthly}{Average\ Temperature}\right) - \left(\underset{Annualy}{Average\ Temperature}\right) \quad (2)$$

ISSN 2523-2881

Table 2 shows the AOs in the city of Queretaro, Mexico, corresponding to the closest meteorological temperatures to the Queretaro International Airport (MMQT).

Month	Average Temperature Monthly (°C)	Average Temperature Annually (°C)	AOs (°C)
January	14	17.362	-3.362
February	16	17.362	-1.362
March	19	17.362	1.638
April	20	17.362	2.638
May	20	17.362	2.638
June	19	17.362	1.638
July	19	17.362	1.638
August	19	17.362	1.638
September	18	17.362	0.638
October	17	17.362	-0.362
November	15	17.362	-2.362
December	14	17.362	-3.362
Average	17.362	17.362	

Table 2 Annual Oscillation of Surface Temperature.

The AOs is obtained by taking the interval between upper and lower values in Graph 2.

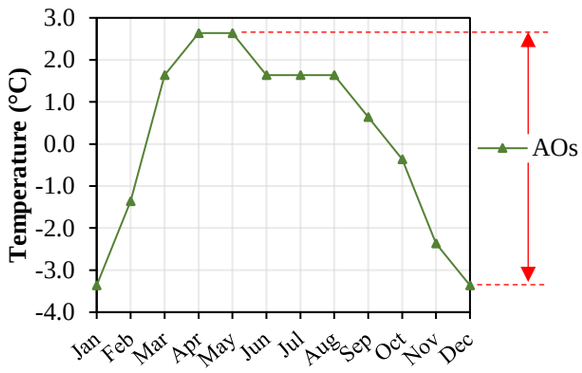

Graph 2 Overall behavior of the AOs in the city of Queretaro, Mexico

2.4. Evolution of the subsoil temperature at different depths

Considering a homogeneous and isotropic Vertisol type soil with constant thermophysical properties, the temperature at any depth Z can be calculated in a time t. Then, the internal temperature of subsoil at different depths is calculated by using Equation 3 (Kusuda & Achenbach, 1965) and data from Graph 1.

$$T(Z,t) = T_m - OA_S \cdot e^{-Z\sqrt{\frac{\pi}{365\cdot\alpha}}} cos\left[\frac{2\pi}{365}\left(t - t_0 - \frac{Z}{2}\sqrt{\frac{365}{\pi\alpha}}\right)\right] \quad (3)$$

A depth interval is selected from 0 to 6 m, and by using Table 1 values as input for Equation 3, the temperature of subsoil is calculated.

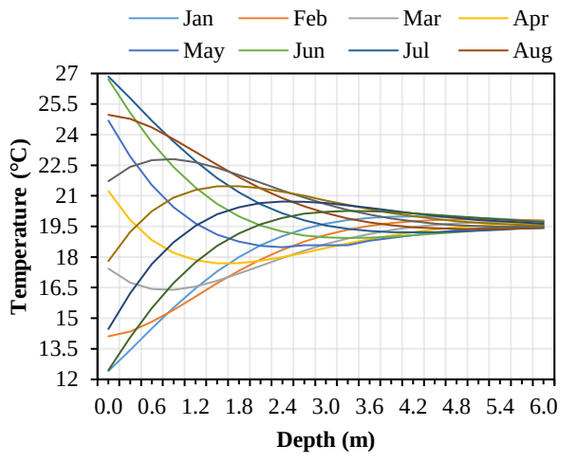

Graph 3 Behavior of internal temperature of subsoil

Graph 3 indicates there is a greater temperature difference on the ground's surface in the months of January - July (Sossa & Sebastián, 2013). and this temperature difference decreases with increasing depth in the subsoil.

3. Results

3.1. Experimental tests at the CGHE and HGHE

Five tests were carried out considering the two boundary conditions mentioned before (see Figures 2 and 3) as well as five simulations in ANSYS-FLUENT for each heat exchanger. The first and second runs were chosen to be analyzed. The first test was performed using water as a refrigerant at 7.35 °C and the second test was similar but at 60.05 °C.

Table 3 shows the temperature results of the 1st and 2nd experimental tests conducted at the CGHE and HGHE.

Test No.	Inlet Temp. (CGHE)	Outlet Temp. (CGHE)	ΔT (°C) (CGHE)
1	7.35 °C	8.62 °C	ΔT = 1.27 °C
2	60.05 °C	57.12 °C	ΔT = 2.96 °C
Test No.	**Inlet Temp. (HGHE)**	**Outlet Temp. (HGHE)**	**ΔT (°C) (HGHE)**
1	7.35 °C	7.95 °C	ΔT = 0.6 °C
2	60.05 °C	57.75 °C	ΔT = 2.24 °C

Table 3 Temperatures of the refrigerant fluid in the 1st and 2nd experimental tests

Graph 4 shows that the CGHE presents a higher ΔT than the HGHE in both tests.

ISSN 2523-2881

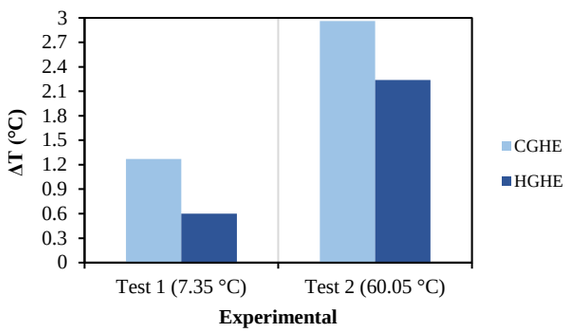

Graph 4 Comparison of experimental ΔT at the CGHE and HGHE

3.2. Boundary conditions in CFD simulations for the CGHE and for the HGHE

The boundary conditions established in the ANSYS-FLUENT simulations are described as follows and can be reviewed in the Figure 7:

- Subsoil temperature profile (Graph 3).
- Vertisol type soil thermal properties (Table 1).
- Thermal properties of PEAD4710.
- Temperature of the refrigerant fluid (water) at 7.35 °C and 60.05 °C.
- Thermophysical properties of the refrigerant fluid (water) at 7.35 °C and 60.05 °C.
- Mass flow rate of the refrigerant fluid.
- Velocity of the refrigerant fluid inside the CGHE and HGHE.

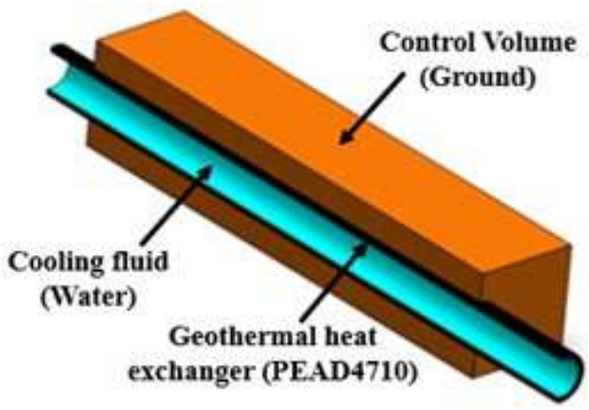

Figure 7. Cross section view of the domain used for setting the boundary conditions in Ansys for CGHE and HGHE

3.3. Results of the numerical simulation of the refrigerant fluid inside the CGHE at a temperature of 7.35 °C

Test 1 was chosen using water as a refrigerant fluid at a temperature of 7.35 °C. Figure 8 depicts the distribution of the temperature inside the CGHE.

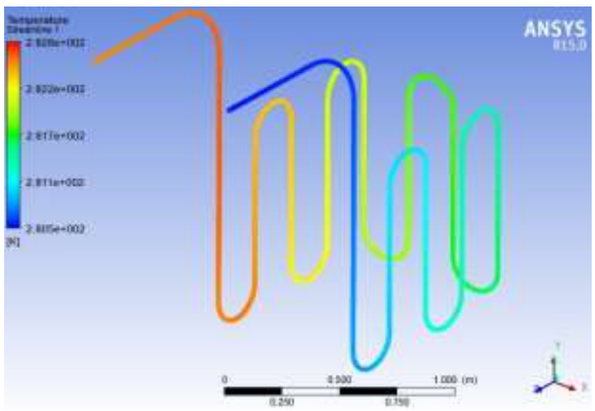

Figure 8 Temperature distribution of the refrigerant fluid inside the CGHE through test 1 at 7.35 °C

3.4. Numerical simulation of the refrigerant fluid inside the CGHE at a temperature of 60.05 °C

Test 2 was chosen using water as a refrigerant fluid at a temperature of 60.05 °C. Figure 9 depicts the distribution of the temperature inside the CGHE.

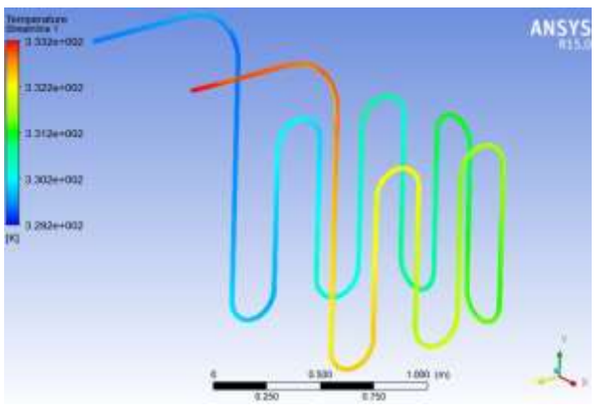

Figure 9 Temperature distribution of the refrigerant fluid inside the CGHE through test 2 at 60.05 °C

3.5. Numerical simulation of the refrigerant fluid inside the HGHE at a temperature of 7.35 °C

Test 1 was chosen using water as a refrigerant fluid at a temperature of 7.35 °C. Figure 10 depicts the distribution of the temperature inside the HGHE.

ISSN 2523-2881

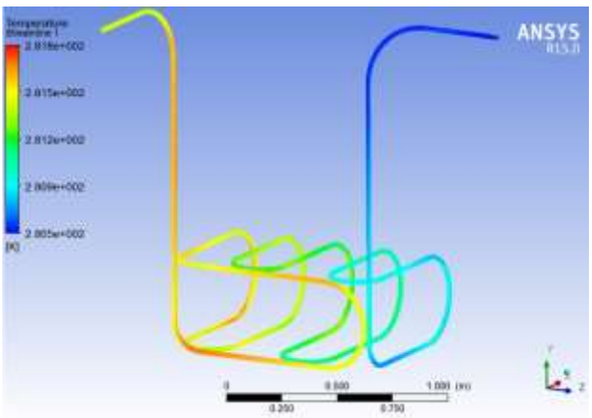

Figure 10 Temperature distribution of the refrigerant fluid inside the HGHE through test 1 at 7.35 °C.

3.6. Numerical simulation of the refrigerant fluid inside the HGHE at a temperature of 60.05 °C

Test 2 was chosen using water as a refrigerant fluid at a temperature of 60.05 °C. Figure 11 depicts the distribution of the temperature inside the HGHE.

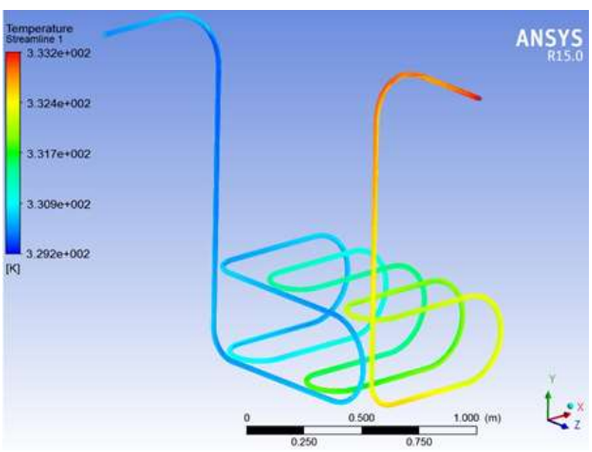

Figure 11. Temperature distribution of the refrigerant fluid inside the HGHE through test 2 at 60.05 °C.

Table 4 describes the results obtained in the ANSYS-FLUENT simulations for tests 1 and 2.

Test No.	Inlet Temp. (CGHE)	Outlet Temp. (CGHE)	ΔT (°C) (CGHE)
1	7.35 °C	9.65 °C	ΔT = 2.3 °C
2	60.05 °C	55.87 °C	ΔT = 4.18 °C
Test No.	**Inlet Temp. (HGHE)**	**Outlet Temp. (HGHE)**	**ΔT (°C) (HGHE)**
1	7.35 °C	8.65 °C	ΔT = 1.3 °C
2	60.05 °C	56.05 °C	ΔT = 4.0 °C

Table 4 Temperatures of the refrigerant fluid in the 1st and 2nd numerical tests.

Graph 5 shows that the CGHE presents a higher ΔT than HGHE just in the 1st test.

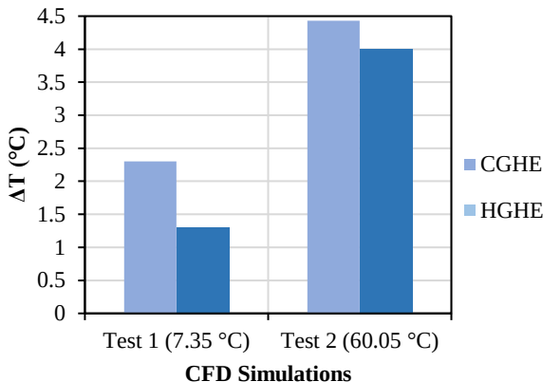

Graph 5 Comparison of numerical ΔT at the CGHE and HGHE.

3.7. Comparative analysis CGHE vs HGHE

The temperature distribution of the refrigerant fluid studied with ANSYS-FLUENT was monitored at different points of the geometry for the CGHE and HGHE for intervals of length equal to 2.25 m considering both tests 1 and 2.

Thus, Graph 6 shows the variation of temperature of the refrigerant fluid at different positions of the CGHE and HGHE geometries at an inlet temperature of 7.35 °C.

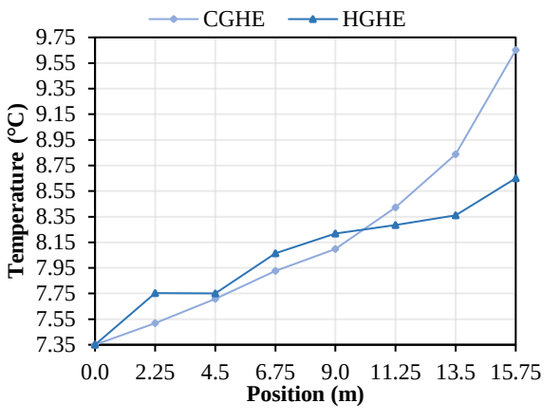

Graph 6 Comparative analysis (7.35 °C): CGHE vs HGHE.

The behavior of the temperature of the refrigerant fluid throughout the position is similar for both exchangers in terms of magnitude, however, in the final positions the CGHE exchanger is considerably separated from the HGHE, see Graph 6. These results correspond to the inlet temperature of 7.35 °C. The temperature in the CGHE is approximately linear while in the HGHE this is lost.

ISSN 2523-2881

The behavior of the temperature of the refrigerant fluid throughout the position is similar for both exchangers in terms of magnitude, however, in the final positions the HGHE exchanger is considerably separated from the CGHE, see Graph 7. These results correspond to the inlet temperature of 60.05 °C. Both exchangers behaved decreasing linearly.

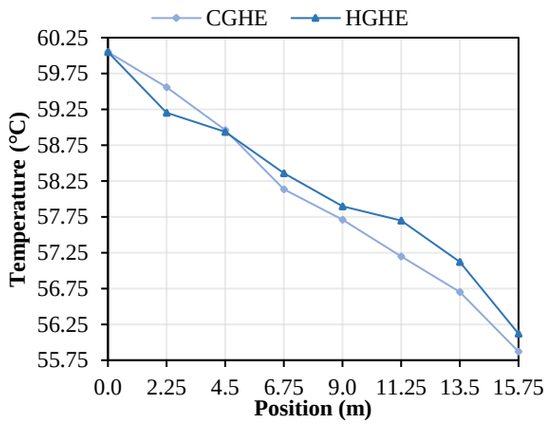

Graph 7 Comparative analysis (60.05 °C): CGHE vs HGHE.

4. Acknowledgements

The authors thank the Center for Engineering and Industrial Development (CIDESI) for the facilities provided to carry out the experimentation and the Polytechnic University of Queretaro (UPQ) for its support and funding of the work.

5. Conclusions

Based on data in Table 4 for ΔT, the following can be concluded:

1. In test 1 where the refrigerant fluid (water) had an inlet temperature of 7.35 °C, the ΔT had a 52.76% greater difference in the CGHE in relation to the HGHE.

2. In test 2 with the refrigerant (water) at the inlet at 60.05 °C, the ΔT had a 24.33% greater difference in the CGHE in relation to the HGHE.

From the experiments and the simulations in ANSYS-FLUENT for the CGHE model, the following can be concluded:

1. The results of experimental test 1 and numerical simulation 1 only presented a temperature difference equal to 1.03 °C.

2. The results of experimental test 2 and numerical simulation 2 only presented a temperature difference equal to 1.22 °C.

3. The refrigerant temperature for the CGHE model behaved practically linear in both tests, with the temperature at the inlet of the refrigerant fluid at 7.35 °C and 60.05 °C, respectively. This behavior is not observed in the same way for the HGHE model, where it was mostly non-linear.

From the experiments and the simulations in ANSYS-FLUENT for the HGHE model, the following can be concluded:

1. The results of experimental test 1 and numerical simulation 1 only presented a temperature difference equal to 0.7 °C.

2. The results of experimental test 2 and numerical simulation 2 only presented a temperature difference equal to 1.76 °C.

6. References

Benli, H. & Durmus, A. (2009). Evaluation of ground-source heat pump combined latent heat storage system performance in greenhouse heating. *Energy and Buildings*, 41(2), 220-228. https://doi.org/10.1016/j.enbuild.2008.09.004

Bose, J., Parker, J. & McQuiston, F. (1985). *Design/data manual for closed-loop ground coupled heat pump systems*. Oklahoma State Univ for ASHRAE

Chen, J., Yang, L. & An, B. (2022). Unsteady analysis of the cold energy storage heat exchanger in a liquid air energy storage system. *Applied Energy*. 87(1), 16 – 27. https://doi.org/10.1016/j.apenergy.2009.04.038

Consejo de Ciencia y Tecnología del Estado de Querétaro (2002). *Uso Actual y Potencial del Suelo en los Municipios conurbados de Querétaro.* [PDF]. Disponible en: http://www.concyteq.edu.mx/concyteq//uploads/publicacionArchivo/2017-06-212.pdf

Eskilson, P. (1987). *Thermal analysis of heat extraction boreholes.* University of Lund. [PDF].

ISSN 2523-2881

Fundación de la Energía de la Comunidad de Madrid (2010). *Guía de la Energía Geotérmica. Dirección General de Industria, Energía y Minas*. Universidad Politécnica de Madrid, [PDF]. Disponible en: https://www.fenercom.com/wp-content/uploads/2008/01/Guia-de-la-Energia-Geotermica-fenercom-2008.pdf

Gong, Q., Yu, C., Wang, W. & Wang, Y. (2023). Experimental and numerical exploration on improved heat transfer by continuous spiral flow in shell of spiral wound corrugated tube heat exchanger, *International Journal of Thermal Sciences*, 191(), https://doi.org/10.1016/j.csite.2023.103483

Guo, L., Zhu, J. & Li, M. (2014). Research and prospect of enhanced heat transfer elements in inter-wall heat exchangers, Guangdong. *Chemical Industry*, 41, 101–107.

INEGI (2007). Marco Geo estadístico Municipal, conjunto de datos vectorial - edafológico, información topográfica digital. Disponible en: https://www.inegi.org.mx/app/biblioteca/ficha.html?upc=889463496731

INEGI (2021). *Aspectos geográficos: Querétaro.* [PDF]. Disponible en: https://www.inegi.org.mx/contenidos/app/areasgeograficas/resumen/resumen_22.pdf

Ingersoll, L. R., Adler, F. T., Plass, H. J. &Ingersoll, A. C. (1950). Theory of Earth Heat Exchangers for the Heat Pump. *Scientific Research Publishing Inc.* 56, 167-188. Available in: https://www.scirp.org/(S(351jmbntv-nsjt1aadkposzje))/reference/referencespapers.aspx?referenceid=682252

International Ground Source Heat Pump Association (2013). *Closed-loop/ground-source heat pump systems – Installation guide*. Oklahoma State University. Available in: https://geoconnectionsinc.com/resources/downloads/IGSHPA_Design_Installation_Standards.pdf

Kusuda, T. & Achenbach, P.R. (1965). *Earth temperature and thermal diffusivity at selected stations in the United States*. [PDF]. Available in: https://nvlpubs.nist.gov/nistpubs/Legacy/RPT/nbsreport8972.pdf

Lv, M., Yang, X. & Zhang, Y. (2018). Analysis of the current situation of heat exchangers and their classification and application. *Chemical Industry*. 47, 582–584.

Meteored (2023). *Histórico del clima en Querétaro.* Disponible en: https://www.meteored.mx/queretaro/historico

Mustafa, O. (2008). Ground-source heat pumps systems and applications. *Renewable and Sustainable Energy Reviews*, 12(2), 344-371. https://doi.org/10.1016/j.rser.2006.10.003

Philippe, M., Bernier, M., Marchio, D. & Lopez, S. (2011). A semi-analytical model for serpentine horizontal ground heat exchangers. *HVAC&R Research*, 17(6), 1044–1058. https://doi.org/10.1080/10789669.2011.607880
Rees, S. (2016). Advances in Ground Source Heat Pump Systems. https://doi.org/10.1016/C2014-0-03840-3

Rousseau, C., Comlan, F., Lamarche, L., Ouzzane, M. & Kajl, S. (2017). Modeling and experimental validation of a transient direct expansion geothermal heat exchanger. *Geothermics*, https://doi.org/10.1016/j.geothermics.2015.06.007

Sossa, V. & Sebastián, M. (2013). *Diseño e integración de energía geotérmica de baja entalpía aplicada a proyectos de construcción residencial*. Universidad de Chile. Disponible en: https://repositorio.uchile.cl/handle/2250/113790 The International Ground Source Heat Pump Association 2nd IGSHPA Research Track was hosted by IGSHPA Sweden and KTH. (2018 September 18-19). Stockholm, Sweden.

Triki, R., Hassene, D. & Baccar, M. (2021). Numerical investigation of heat treatment of an olive paste within a scraped surface heat exchanger equipped with helix screw. *Arabian Journal of Geosciences*, 14(2180), https://doi.org/10.1007/s12517-021-08535-9

Yang, H., Cui, P. & Fang, Z. (2009). Vertical-borehole ground-coupled heat pumps: a review of models and systems. *Applied Energy*, 87 (1), 16–27. https://doi.org/10.1016/j.apenergy.2009.04.038

ISSN 2523-2881

Zheng, G., Xiao, Q., Zhu, S., Wang, H., Geng, J., Zhao, S. & Huang, J. (2022). Analysis of heat transfer performance of ORC direct contact heat exchanger by GRA-VMD-LSSVM model using optimization. *Korean Journal of Chemical Engineering,* 39 () 1729–1743, https://doi.org/10.1007/s11814-022-1080-9

ISSN 2523-2881